Published in final edited form as:
In Vitro Cell Dev Biol Anim. 2002 ; 38(10): 582–594.

NOVEL COMPLEX INTEGRATING MITOCHONDRIA AND THE MICROTUBULAR CYTOSKELETON WITH CHROMOSOME REMODELING AND TUMOR SUPPRESSOR RASSF1 DEDUCED BY IN SILICO HOMOLOGY ANALYSIS, INTERACTION CLONING IN YEAST, AND COLOCALIZATION IN CULTURED CELLS

LEYUAN LIU, **AMY VO**, **GUOQIN LIU**, and **WALLACE L. MCKEEHAN**[1,2]
Center for Cancer Biology and Nutrition, Institute of Biosciences and Technology, Texas A&M University System Health Science Center, 2121 W. Holcombe Boulevard, Houston, Texas 77030 (L. L., A. V., W. L. M.) and State Key Laboratory of Plant Physiology and Biochemistry, College of Biological Sciences, China Agricultural University, Beijing 100094 P.R. China (G. L)

Summary

Availability of the complete sequence of the human genome and sequence homology analysis has accelerated new protein discovery and clues to protein function. Protein–protein interaction cloning suggests multisubunit complexes and pathways. Here, we combine these molecular approaches with cultured cell colocalization analysis to suggest a novel complex and a pathway that integrate the mitochondrial location and the microtubular cytoskeleton with chromosome remodeling, apoptosis, and tumor suppression based on a novel leucine-rich pentatricopeptide repeat-motif–containing protein (LRPPRC) that copurified with the fibroblast growth factor receptor complex. One round of interaction cloning and sequence homology analysis defined a primary LRPPRC complex with novel subunits cat eye syndrome chromosome region candidate 2 (CECR2), ubiquitously expressed transcript (UXT), and chromosome 19 open reading frames 5 (C19ORF5) but still of unknown function. Immuno, deoxyribonucleic acid (DNA), and green fluorescent protein (GFP) tag colocalization analyses revealed that LRPPRC appears in both cytosol and nuclei of cultured cells, colocalizes with mitochondria and β-tubulin rather than with α-actin in the cytosol of interphase cells, and exhibits phase-dependent organization around separating chromosomes in mitotic cells. GFP–tagged CECR2B was strictly nuclear and colocalized with condensed DNA in apoptotic cells. GFP–tagged UXT and GFP–tagged C19ORF5 appeared in both cytosol and nuclei and colocalized with LRPPRC and β-tubulin. Cells exhibiting nuclear C19ORF5 were apoptotic. Screening for interactive substrates with the primary LRPPRC substrates in the human liver complementary DNA library revealed that CECR2B interacted with chromatin-associated TFIID-associated protein TAFII30 and ribonucleic acid splicing factor SRP40, UXT bridged to CBP/p300–binding factor CITED2 and kinetochore-associated factor BUB3, and C19ORF5 complexed with mitochondria-associated NADH dehydrogenase I and cytochrome *c* oxidase I. C19ORF5 also interacted with RASSF1, providing a bridge to apoptosis and tumor suppression.

[1]To whom correspondence should be addressed at wmckeeha@ibt.tamu.edu.
[2]All figures from this manuscript are published in color online and may be viewed at http://inva.allenpress.com/invaonline/?request=index-html

Keywords

apoptosis; chromosome separation; cytokinesis; genetic instability; microtubule-associated proteins; nucleo-cytosolic shuttling; tumor suppressor

Introduction

Availability of the complete sequence of the human genome has greatly accelerated the deduction of the complete sequence and genetic information concerning new proteins. Deduction of the molecular and cellular functions then becomes a major challenge. In the absence of a clear functional homologue identified by overall sequence, reiterative approaches in silico of increasing sophistication can be used to identify functional motifs and structural homology domains of proteins of known function as clues to biochemical function (Thornton, 2001). Leucine-rich pentatricopeptide repeat-motif–containing protein (LRPPRC, previously called gp130 or LRP130) (M92439) was first identified in detergent extracts of differentiated human hepatoma cells (HepG2) enriched for complexes of ligand-labeled fibroblast growth factor receptor (FGFR) (DiSorbo et al., 1988). Cloning and deduced sequence revealed a 4782-bp complementary deoxyribonucleic acid (cDNA) from human chromosome 2 (Ghiso and Lennon, 1994), coding for a leucine-rich intracellular protein of 130 kDa with no apparent functional homo-logues (Hou et al., 1994). The mouse homologue of LRPPRC was reported subsequently among retinoic acid–responsive transcripts that were differentially expressed within 48 h after treatment of P19 embryonic carcinoma cells to induce neuronal differentiation (Suzuki et al., 1995). Advances in detection and sequencing components in multiprotein complexes have revealed the presence of LRPPRC sequences in diverse complexes derived from mammalian cell sources in addition to the FGFR complex (Liu and McKeehan, 2002). The common functional feature of principal components of these diverse complexes is a direct or indirect association with cell membranes and the cell cytoskeleton in the cytosol and DNA and ribonucleic acid (RNA) in the nucleus. A sequence domain homology analysis using bioinformatic discovery tools, revealed that LRPPRC comprises clusters of a total of 23 α-helical repeats that are distinct but similar to PPR, tetratricopeptide, and Huntingtin-Elongation-A subunit-TOR (HEAT) repeats (Liu and McKeehan, 2002). The N-terminal half of LRPPRC exhibits multiple copies of potential LXXLXL nuclear export signals and an epsin 1 N-terminal homology (ENTH) domain between clusters of leucine-rich repeats (LRP). The C-terminal half exhibits the domain of unknown function 28 (DUF28) and the secretory 1 (SEC1) structural homology domain. The homology domain structure of LRPPRC is consistent with both cytosolic and nuclear location and function, including nucleocytosolic translocation and a role in vesicular transport and organelle reorganization.

Interaction cloning approaches, as the yeast two-hybrid system (Fields and Song, 1989), provide a tool to derive further clues about protein function by direct association, particularly if the interaction occurs with a partner of well-characterized function. Motif and structural homology domain analyses of interactive partners of unknown function may also yield further clues. Screening of a human liver cDNA library using subdomains of LRPPRC as bait in the yeast two-hybrid system revealed that the SEC1 domain, in particular, interacted directly with microtubule (MT)–associated protein (MAP) homologue C19ORF5 (XP_038600) and UXT (XP_033860) (Liu and McKeehan, 2002). Unfortunately, all three direct-acting partners were also of largely unknown function. However, motif and sequence domain analyses of both primary substrates suggested homology domains to proteins with known cytoskeletal associations in experimental biological systems. UXT also exhibited subdomains homologous to those in certain transcription factors. A third SEC1 domain–interactive substrate, CECR2B (AF411609), exhibited homology domains with known

proteins that are associated with both the microtubular cytoskeleton and chromatin (Liu and McKeehan, 2002).

In this report, we used cultured cells in vitro to determine the subcellular distribution and colocalization of LRPPRC and its primary SEC1 domain substrates C19ORF5, UXT, and CECR2 by immunocytochemistry and expression of green fluorescent protein (GFP)–tagged recombinant products. In interphase cells, cytosolic LRPPRC colocalized with β-tubulin, which is indicative of a potential MT association instead of the actin cytoskeleton and, surprisingly, mitochondria. Moreover, LRPPRC exhibited phase-dependent organization around separating chromosomes in mitotic cells. Expression of GFP-tagged LRPPRC and substrates UXT and C19ORF5 confirmed that all three are likely associated with the MT cytoskeleton in the cytosol in healthy cells, whereas GFP-tagged CECR2B was solely nuclear. Nuclear GFP–C19ORF5 appeared only in apoptotic cells and in apoptotic nuclei, whereas both GFP–C19ORF5 and GFP–CECR2B were associated with condensed, deteriorating DNA. These results buttressed the prediction of an association of LRPPRC or its primary associates with the MT cytoskeleton and nucleic acid and both the cytosolic and nuclear locations predicted by in silico motif and homology domain analyses. The in vitro cellular association screen suggested a role for the LRPPRC complex in chromosome remodeling and cytokinesis during mitosis. Moreover, the cellular association results unexpectedly revealed a mitochondrial association and potential role in apoptosis not apparent from the interaction cloning and the in silico homology analyses.

Finally, because primary LRPPRC-interactive substrates revealed by interaction cloning were of unknown function, we performed a secondary screening of the same human liver cDNA expression library using primary substrates UXT, CECR2B, and C19ORF5 as capture bait. The results revealed interactive substrates of known function that bridge to transcription complexes, the kinetochore complex, the apoptotic tumor suppressor RASSF1, and mitochondrial complexes I and IV. These combined results were used to build a novel hypothetical complex that integrates mitochondria and the microtubular cytoskeleton with chromosome remodeling and apoptotic tumor suppression.

Materials and Methods

GFP constructs

A 4.7-kb pEGFP-C3 vector (CLONTECH Laboratories, Inc., Palo Alto, CA) was used to fuse GFP at the N terminus. A cDNA coding for GFP–LRPPRC, with GFP fused at leucine 18 of full-length LRPPRC (Liu and McKeehan, 2002), was created by ligation of the pEGFP-C3 vector cut with *Hin*dIII and *Kpn*I, a 1.75-kb *Hin*dIII and *Sal*I fragment from LRP130-pBluescript SK and a 2.0-kb *Sal*I–*Kpn*I fragment from a LRP130-GST-pBluescript SK engineered with a *Kpn*I site at the exact end of the LRPPRC coding sequence. GFP–CECR2B was the ligation product of an *Eco*RI-*Sma*I–digested pEGFP-C3 and a 1.5-kb fragment from CECR2B–pACT2 (Liu and McKeehan, 2002) derived by *Sma*I–*Xho*I treatment. The *Xho*I end was filled with Klenow fragment of DNA polymerase I and then cut with *Eco*RI. For construction of GFP–UXT, pEGFP-C3 was cut with *Kpn*I, and the UXT gene was amplified by polymerase chain reaction (PCR) from the UXT–pACT2 template (Liu and McKeehan, 2002) using primers CATGCGAATTCATGGCGACGC and CACTTGGATCCATATGGTGAGGCTTCTC. After digestion with *Bam*HI and *Eco*RI and filling to yield blunt ends, the two fragments were ligated. GFP–C19ORF5 was the ligation product of *Eco*RI-*Sma*I–digested pEGFP-C3 and a 1.3-kb fragment from C19ORF5–pACT2 (Liu and McKeehan, 2002). The latter coded for the C-terminal 393 residues of the 672-residue C19ORF5 and was derived by *Nco*I–*Bgl*II digestion, filled with Klenow fragment, and cut with *Eco*RI for ligation.

Cell culture

About 2.5×10^5 COS7 or HepG2 cells were plated on 22-mm^2 coverslips coated with 10 μg/ml of solubilized collagen (Vitrogen from Nutacon, Leimuiden, The Netherlands) in six-well plates. Cells were maintained in RD medium supplemented with 5% fetal bovine serum (FBS) in humidified 95% air and 5% CO_2 overnight at 37° C. The RD medium was comprised of 5.2 g/L RPMI medium 1640, 6.7 g/L Dulbecco modified Eagle medium (Invitrogen Life Technologies, Carlsbad, CA), 3.3 g/L of *N*-2-hydroxyethyl-piperazine-*N*′-2-ethane-sulfonic acid, 110 mg/L of Na-pyruvate, 14 g/L Na-HCO_3, and 100 mg/L of kanamycin. After incubation overnight, the cells were fixed for immunostaining for endogenous LRPPRC or used for transient transfection of GFP fusion constructs. To increase the number of cells in mitosis for observation of LRPPRC and substrates in the division cycle, cells were starved for 16 h without serum and stimulated with 5% FBS for 4 h before fixation. For the mitochondrial colocalizations, cells were exposed to 1 μ*M* of MitoTracker® Red CM-H_2XRos (Molecular Probes, Inc., Eugene, OR) for 30 min before fixation. Cells were exposed for 24 h to 10 μ*M* of nocodazole or taxol (Sigma-Aldrich, St. Louis, MO) before analysis, as indicated in the text.

Expression of GFP fusion proteins

Transient transfection of GFP fusion proteins using liposome transfer was carried out according to the manufacturer's recommendations (Invitrogen Life Technologies). Transfection conditions were first optimized for cell density, type of liposome reagent, liposome volume, transfected DNA, time of exposure to liposomes, and incubation time and conditions between liposome removal and analysis based on fluorescence with the pEGFP-C3 vector alone. On average, about 2 μg plasmid DNA was mixed with 5 μl of CELLFECTIN™ or LIPOFECTAMINE™ (Invitrogen Life Technologies) in a total volume of 200 μl serum-free RD without kanamycin and was held at room temperature for 30 min. The mixture was then diluted into 1 ml serum-free RD without kanamycin. One milliliter RD medium with 10% FBS was added to the mixture 4 h after transfection and left overnight. The mixture was replaced with 2 ml fresh RD medium with 5% FBS, and the cells were incubated for another 24 to 72 h before analysis. Individual transfected cells were visibly apparent among the surrounding untransfected cells that served as internal untransfected controls. Transfection efficiency was estimated by visual observation to be about 30%.

Fixation, immunofluorescence, microscopy, and image capture

Cells were fixed and permeabilized for fluorescence analysis after washing twice for 5 min with 1× phosphate-buffered saline (PBS), as described by Goold et al. (Goold and Gordon-Weeks, 2001). After treatment for 10 min with 4% paraformaldehyde (Sigma-Aldrich) at room temperature, cells were permeabilized by treatment for 5 min with 0.1% Triton X-100 (Bio-Rad, Hercules, CA). Cells were stained for 1 min with 4 μg/ml of 4,6-diamidino-2-phenylindole (DAPI, Sigma-Aldrich), and the coverslips were mounted and sealed in Aqua Poly/Mount (Polysciences, Inc., Warrington, PA) for direct fluorescence analysis. For indirect immunofluorescent staining, permeabilized cells were treated for 30 min with 0.2% bovine serum albumin (BSA, Sigma-Aldrich) in 1× PBS to reduce nonspecific binding. After the block solution was removed, cells were treated with 50 μl of either mouse monoclonal anti-LRPPRC antibody Mab4C12 (a gift from Dr. Serafín Piñol-Roma, Mount Sinai School of Medicine, New York) or mouse monoclonal anti-β-tubulin (clone TUB 2.1) (Sigma-Aldrich). The reactive epitope for Mab4C12 has been mapped to a sequence between amino acid residues 500 and 600 of LRPPRC by immunoprecipitation of deletion constructs synthesized by in vitro transcription–translation and by immunoblots of constructs expressed in *Escherichia coli* (S. Mili and S. Pinol-Roma, pers. comm.). The antibody-containing solution was applied to cells in the center of a coverslip that was placed

at the center of the cultures and was held at room temperature for 1 h. The coverslip was then washed twice for 5 min with 1× PBS and blocked again with 0.2% BSA in 1× PBS. Fifty microliters of diluted secondary antibody was applied to the center of the coverslip, and the coverslip was kept at room temperature for 1 h. The secondary antibody was Texas Red®-X goat anti-mouse IgG (Molecular Probes) to contrast with GFP- or fluorescein isothiocyanate–conjugated goat anti-mouse IgG (Santa Cruz Biotechnology, Santa Cruz, CA) to contrast with MitoTracker® Red CM-H_2XRos. Finally, the coverslip was washed twice for 5 min with 1× PBS, counterstained with DAPI, and mounted and sealed for microscopic analysis. Antibodies used were affinity-purified Ig fractions. Optimum dilutions were determined for the maximum positive signal to background ratios. For actin staining, one unit of Texas Red-X–labeled phalloidin (Molecular Probes) in 50 μl 1× PBS was added to cells for 30 min, which were fixed and permeabilized as described above.

Under the control of UltraView software, fluorescence was elicited with SpectraMASTER;, and images were captured by an UltraPix camera system through an Olympus IX70 inverted scope using a ×40/1.35 oil iris (Olympus America Life Science Resources Ltd., Melville, NY). The images captured at different excitation wavelengths were assigned different colors and merged to determine the overlap of signals. For example, GFP and mitochondria were assigned green; LRPPRC, β-tubulin, and F-actin red; and DNA blue in all except Fig. 2. The combined images were exported as tiff files and further refined with Adobe Photoshop® version 5.5 (Adobe, San Jose, CA).

Identification of interactive partners in the yeast two-hybrid system

The three primary SEC1 domain–interactive LRPPRC substrates CECR2B, UXT, and C19ORF5 were identified, validated, and analyzed by sequence domain homology as described by Liu and McKeehan (2002). Interactive substrates for the primary substrates were identified in the described yeast two-hybrid capture system using the same human liver cDNA library. Fusions to coding sequence for the yeast DNA-binding domain were constructed by ligating the CECR2B, UXT, or C19ORF5 cDNA in frame with the DNA-binding domain–coding sequence in the pGBKT7 vector. CECR2B–pGBKT7 was derived by the ligation of *Nde*I-*Sma*I–digested pGBKT7 and a 1.2-kb *Nde*I–*Pvu*II fragment excised from CECR2B–pACT2 (Liu and McKeehan, 2002). UXT–pGBKT7 was created by ligation of the *Bam*HI-*Eco*RI–digested pGBKT7 vector and the PCR-generated fragment from UXT–pACT2, using the same primers as those described earlier for the construction of GFP–UXT. C19ORF5–pGBKT7 was created by ligation of *Nco*I-*Pst*I–digested pGBKT7 and C19ORF5–pACT2. The coding sequence spanned aspartate 279 to glutamine 620 that exhibited both a potential messenger RNA (mRNA) and an MT-binding domain predicted by homology (Liu and McKeehan, 2002). Each pGBKT7 construct was used as bait to trap interactive substrates during a screen of a human liver cDNA library carried by pACT2 vector as described by Liu and McKeehan (2002). The positive clones for each screening were confirmed by retesting the trap-protein interaction based on the ability of cotransformants of the interaction trap and library-derived DNA plasmids in AH109 to grow on quadruple dropout (QDO) selection plates. The positive colonies were sequenced and confirmed to be in the same reading frame with the transcription activation domain. As a control, plasmid pGBKT7 carrying only the DNA-binding domain was cotransformed with plasmids carrying activation domain–fused substrates into AH109. The cotransformants were unable to grow on QDO selection plates, which verified that the substrates activate reporter genes through interaction with the fusion bait.

RESULTS

Distribution of LRPPRC antigen in interphase cells

Indirect immunofluorescent staining of COS7 cells from monolayer cultures of about 2.5×10^5 cells with a mouse monoclonal antibody (Mab4C12) directed against a recombinant fragment of LRPPRC (Materials and Methods) revealed two general staining patterns. In 10% of about 2000 cells observed in 100 different fields, Mab4C12 yielded predominantly an extranuclear staining pattern in which nuclei were practically clear (type I pattern) (Fig. 1*A*). Mab4C12 antigen appeared to colocalize and organize with cytoskeletal structures that were most intense beginning in the perinuclear region but swirled outward toward the cell periphery and, in rounded cells, sometimes covered the entire cell to the periphery (not shown). In the other 90% of cells (type II pattern), the presumed LRPPRC antigen was condensed within a much smaller perimeter around the nucleus, with possibly some antigen in the nucleus. The stain throughout the cytosol exhibited less organization and appeared in a punctate pattern in some areas (Fig. 1*B*). Examination of multinucleate cells that constituted less than 5% of the population further illustrated the intense staining around and between nuclei (Fig. 1*C* and *D*). In contrast to COS cells, the Mab4C12 stain in the HepG2 cell line, in which LRPPRC was discovered, exhibited an extranuclear punctate pattern that constituted 100% of the 2000 interphase cells examined in about 100 fields (Fig. 1*E*).

Distribution of LRPPRC antigen in mitotic cells

Despite the different staining patterns of LRPPRC antigen in interphase COS7 and HepG2 cells, the profile in mitotic cells in both cultures was remarkably similar (Fig. 2). Cells in mitosis were examined in COS7 (not shown) and HepG2 (Fig. 2) cultures after increasing the mitotic cell population to about 1% by exposure to serum after 16 h in serum-free medium. Cultures were stained with anti-LRPPRC Mab4C12 (*red*), counterstained with DAPI (assigned *green*), and examined at different stages of mitosis. In prophase cells, LRPPRC antigen appeared associated with and interspersed among condensed chromosomes in no particular pattern (Fig. 2*A*). In metaphase cells, it was relatively clear of the chromosomes at the metaphase plate and dispersed out from the plate to poles in a notable punctate pattern (Fig. 2*B*). In cells in anaphase and telophase after sister chromatids had separated, the punctate pattern diminished, and LRPPRC antigen appeared particularly concentrated between and surrounding the chromatid sets (Fig. 2*C* and *D*). Figure 2*D* shows another cell in anaphase, in which there is an apparent fragment of DNA or lagging chromosome between the two main chromatids. Pincers of LRPPRC antigen appeared to envelope the isolated DNA from multiple directions, similar to the whole chromatids. In telophase cells, two distinct rings of LRPPRC antigen encircled each set of daughter chromatids associated with the developing daughter cells, presumably where new nuclear membranes will form.

LRPPRC antigen is associated with mitochondria in interphase cells

The punctate staining pattern exhibited by LRPPRC antigen in some areas of the cytosol in interphase COS7 cells (Fig. 1*B*) that predominates in interphase HepG2 cells (Fig. 1*E*) and that is apparent particularly in metaphase of both cell types (Fig. 2*B*) was similar to that reported for mitochondria in other systems (Wang et al., 2000; Collins et al., 2002). To determine whether the Mab4C12 signal colocalized with mitochondria, living cells were treated with MitoTracker® Red CM-H_2XRos (assigned *green*) before staining with Mab4C12 (*red*). The punctate pattern of LRPPRC stain was completely superimposed with the mitochondria reporter in interphase HepG2 cells, where both were concentrated around the nucleus and radiating out to the cell periphery (Fig. 3*A*). In COS7 cells in which the punctate pattern of LRPPRC staining was not dominant (Fig. 1), the *yellow merged* overlay

indicates that LRPPRC overlaps with the punctate mitotracker signal, a pattern that was apparently masked by the total LRPPRC stain in COS7 cells (Fig. 3*B*).

The cytosolic LRPPRC antigen in COS7 cells shown in Fig. 1*A* was suggestive of an association with the MT cytoskeleton, and the antigen was distributed where MT spindle arrays reside in metaphase cells. Because mitochondria have also been shown to be directly or indirectly associated with MT (Heggeness et al., 1978; Karbowski et al., 2001), we treated COS7 cells with the MT-stabilizing drug, taxol, and MT-disrupting drug, nocodazole. The taxol treatment uncovered the punctate staining of LRPPRC in all the 200 COS7 cells observed in treated cultures (Fig. 3*C*), a pattern similar to the one that predominated in HepG2 cells (Fig. 3*A*). Treatment with nocodazole abrogated the distinct distribution pattern observed for both mitochondria and LRPPRC in all the 200 COS7 cells that were observed (Fig. 3*D*).

Colocalization of Mab4C12 antigen with recombinant LRPPRC and effect of expression of recombinant CECR2B, UXT, and C19ORF5

To confirm that the antigen detected by Mab4C12 was LRPPRC, we tested the colocalization of transfected GFP–LRPPRC (*green*) and endogenous Mab4C12 antigen (*red*) (Fig. 4). The GFP portion of GFP–LRPPRC exhibited only the broad extranuclear type of staining exhibited by Mab4C12 characteristic of the COS7 cell type I pattern (Fig. 1*A*) and colocalized with it (Fig. 4*A*). No transfected cells, among over 2000 cells observed, exhibited the type II staining pattern that comprised over 90% of untransfected cells (Figs. 1*B–D* and 4*Cb*). This strongly suggested that the antigen revealed by the Mab4C12 antibody was LRPPRC.

The GFP signal from transfected GFP–CECR2B was strictly nuclear (Fig. 4*B*). Notably, in all of about 200 transfected cells examined, overexpressed CECR2B appeared only in cells exhibiting the type II pattern of LRPPRC display (Fig. 4*B*). Expression of CECR2B appeared to enhance definition of the MT-like structure of the LRPPRC signal that was condensed around and emanating out from the nucleus in the type II pattern (compare Figs. 4*B* and 1*B*). The GFP signal introduced with recombinant UXT appeared to be distributed across the entire cell but was most intense at or in the nucleus in more than 95% of the cells examined (Fig. 4*C*). Of over 1000 cells that were examined that expressed recombinant GFP–UXT, all exhibited the intense nuclear-associated LRPPRC with the less intense cytoskeletal-associated type II pattern in the cytosol (Fig. 1*B–D*). We observed no UXT-transfected cells characteristic of the type I pattern in which nuclear staining of LRPPRC was deficient (Figs. 1*A* and 4*A*). Similar to CECR2B-transfected cells, expression of GFP–UXT also appeared to enhance definition of the MT-like cytoskeletal pattern of LRPPRC extending out from the nucleus. Separate experiments indicated that the foregoing observations were strictly dependent on transfection with GFP fused to cDNAs for the particular LRPPRC substrate. Green fluorescent protein alone gave no distinct patterns.

Cells within the cultures transfected with recombinant GFP–C19ORF5 exhibited an additional degree of heterogeneity with respect to both the transfected GFP reporter and LRPPRC. Ninety percentage of the 1000 cells examined 24 h after transfection exhibited a normal morphology, in which the GFP signal was dispersed relatively uniformly through the cytosol (Fig. 4*D*). Similar to the type I staining pattern for LRPPRC, the nucleus was largely clear of the C19ORF5 signal. However, in all the GFP-C19ORF5–transfected cells, LRPPRC exhibited an intensified nuclear association that was distinct from the two patterns observed in untransfected cells. In about 5% of the GFP-C19ORF5–transfected cells, some areas of punctate staining were apparent within the cytosol, accompanied by an intense perinuclear halo of GFP fluorescence (Fig. 4*Ea*). In these cells, in addition to the intense nuclear association observed in all cells showing GFP–C19ORF5 fluorescence, LRPPRC

exhibited the punctate pattern in the cytosol, suggestive of the mitochondrial distribution shown in Fig. 3 in HepG2 cells and revealed in COS7 cells by treatment with taxol (Fig. 4*Eb*). In the other 5% of the GFP-C19ORF5–transfected cells, colocalized GFP and the LRPPRC signals appeared condensed within the nuclei in round cells or at one edge of the nucleus in elongated cells (Fig. 4*F*). At 72 h after transfection, the last two morphologies that comprised together 10% of the 24-h posttransfection population, increased to about 20% each. The foregoing cell phenotypes were strictly dependent on cells exhibiting green fluorescence, indicating that transfection with GFP fused to C19ORF5. The distinctive green and red fluorescent patterns were not apparent in cells transfected with GFP alone. The nature of the phenotype exhibiting condensed areas of colocalized LRPPRC and C19ORF5 is investigated in more detail in the next section.

Taken together, these results are consistent with predictions from structural homology analysis and preliminary reports from cell extracts (Liu and McKeehan, 2002). Liu and McKeehan (2002) confirm that LRPPRC appears in multiple cellular locations associated with cellular organelles in both cytosol and nuclear compartments, where primary substrates indicated by interaction cloning are present. The impact of overexpression of primary substrates CECR2B, UXT, and C19ORF5 on distribution of LRPPRC, suggests a functional interaction among them.

Nuclear concentration of recombinant GFP–C19ORF5 coincident with LRPPRC accompanies apoptotic phenotypes

As described above, cells exhibiting condensed areas in which C19ORF5 and LRPPRC colocalize in the nucleus increased with time in GFPC19ORF5–transfected cultures (Fig. 4*F*). Examination of green fluorescent GFP-C19ORF5–transfected cells 72 h after transfection exhibiting condensed areas of nuclear-associated C19ORF5 and LRPPRC over a 20-fold range of camera sensitivity settings revealed three general patterns with respect to morphology and intensity of GFP signal (Fig. 5). Figure 5*Aa* shows a binucleate cell in which C19ORF5 was condensed in one nucleus and not the other next to the 60% majority cell type of cells transfected with GFP–C19ORF5 (Fig. 5*BI*). For reference, Fig. 5*Ab* shows the same field at 20-times reduced sensitivity, in which only the nucleus exhibiting the intense GFP signal was visible. The majority of C19ORF5-transfected cell types in which LRPPRC exhibited an intense nuclear association (Fig. 4*D*) exhibited an intact nucleus that stained uniformly with DAPI DNA stain (Fig. 5*BI*). By reducing the sensitivity twice, one class of cells exhibiting condensed nuclear-associated GFP–C19ORF5 was observed, in which the DNA was condensed toward one side of the nucleus and enveloped by the GFP–C19ORF5 in a net-like structure (Fig. 5*BII*). By reducing the sensitivity 10 times, further condensation of DNA that was encircled by C19ORF5 was apparent (Fig. 5*BIII*). When sensitivity was reduced 20 times (Fig. 5*Ab*, 5*BIV*), we observed that the DNA had nearly disappeared in nuclei in which the GFP–C19ORF5 was condensed to the highest density. In contrast, the DNA was largely intact in the adjacent nucleus in binucleate cells in which the nucleus was clear of C19ORF5 (Fig. 5*BIV*). The condensation and fragmentation of nuclear DNA coincident with dissolution of the nuclear membrane and DNA observed here in cells transfected with GFP–C19ORF5 are morphologic hallmarks of apoptosis. The foregoing states were observed only in cells exhibiting green fluorescence, indicating expression of GFP–C19ORF5.

Condensation of nuclear DNA accompanies expression of recombinant GFP–CECR2B

In 90% of cells transfected with GFP–CECR2B, the GFP signal was distributed uniformly in the nuclei (Fig. 4*B*). In about 10% of transfected cells, the GFP signal was notably condensed into one or more areas within a single nucleus (Fig. 6*A*–*Da*). In the same cells, DNA assessed by DAPI stain was similarly condensed (Fig. 6*A*–*Db*) and regionalized in

several patterns, each of which superimposed with GFP–CECR2B (Fig. 6*A*–*Dc*). This morphology that is characteristic of cells in advanced stages of apoptosis (Li et al., 2000) was dependent on transfection of cultures with GFP–CECR2B. No cells exhibiting this characteristic pattern with respect to DNA staining in a total of 2000 cells in 100 fields were detected in untransfected COS7 cell cultures or cultures transfected with empty or GFP-containing vectors.

Recombinant LRPPRC and primary substrates UXT and C19ORF5 colocalize with β-tubulin and not with F-actin

Sequence domain homologies to cytoskeletal-associated proteins (Liu and McKeehan, 2002) and distribution patterns in this report suggest interfaces of LRPPRC and primary substrates UXT and MAP homologue C19ORF5 with cytoskeletal structures. To determine whether LRPPRC and the two primary substrates were associated with elements of the MT or actin cytoskeleton or both in the cytosol of interphase cells, we compared localization of the green signal of the GFP tag at the N-terminus of LRPPRC, UXT, or C19ORF5 with the red signal of the anti-β-tubulin and F-actin stained with Texas Red–conjugated phalloidin in transfected COS7 cells. The GFP signal generally overlapped with the cytosolic anti-β-tubulin stain (Fig. 7), whereas signals from neither of the transfected products overlapped with the phalloidin stain (Fig. 8). Although overexpression of GFP–LRPPRC, GFP–UXT, and GFP–C19ORF5 causes loss in definition of the MT cytoskeleton, presumably because of depolymerization of MT, the selective colocalization with β-tubulin rather than with F-actin suggests that steady-state LRPPRC and cytosolic substrates UXT and C19ORF5 directly or indirectly associate selectively with the MT cytoskeleton.

Secondary substrates of the LRPPRC complex identified by yeast two-hybrid capture

Other than the cellular colocalizations described here and predictions from sequence and structural domain homology, little is known of the function of primary substrates CECR2B, UXT, and C19ORF5 of the LRPPRC SEC1 domain (Liu and McKeehan, 2002). To derive further clues, we screened the same human liver cDNA library in which CECR2B, UXT, and C19ORF5 were identified, using them as bait in the yeast two-hybrid expression system (Table 1). Strictly nuclear CECR2B captured strictly nuclear TATA-binding protein (TBP)–associated factor 30-kDa subunit for RNA polymerase II (TAFII30/TAFIIH; XP_018077) (Jacq et al., 1994) and serine-arginine–rich protein SRP40 (S59042). SRP40 is a member of the highly conserved SRP family involved in alternative splicing and mRNA maturation (Longman et al., 2000). UXT captured the 35-kDa serine-glycine–rich protein P35srj/MRG1 (AAF01263) (Bhattacharya et al., 1999) and the human homologue of kinetochore-associated mitotic checkpoint control protein BUB3 (O43684) (Sudakin et al., 2001). P35srj/MRG1 is the product of the *CITED2* gene (CBP/p300-interacting transactivator with glutamic acid [E]/aspartic acid [D]-rich C-terminal domain 2), so named because of its high affinity for the CH1 region of transcriptional coactivator p300/CBP (Goodman and Smolik, 2000). Last, the MAP homologue C19ORF5 trapped potential tumor suppressor Ras association (RalGDS/AF-6) domain family factor 1 (RASSF1; AAD44175) (Dammann et al., 2000; Vos et al., 2000) and mitochondrial reduced form of nicotinamide adenine dinucleotide (NADH) dehydrogenase subunit 1 (AAL54787) (Hatefi, 1985) and cytochrome *c* oxidase I (COX1) (AAG59851) (Ruitenberg et al., 2002), subunits of complexes I and IV, respectively, of mitochondrial electron transport during oxidative phosphorylation.

Discussion

A hypothetical LRPPRC complex, mitochondria, and the MT cytoskeleton

By combined in silico sequence and structural domain homology analysis, interaction cloning in yeast, and colocalization in cultured cells in vitro, we have described a new

complex that associates with and probably interacts directly or through one or more of its subunits with molecular elements of the MT cytoskeleton and mitochondria. LRPPRC colocalizes with β-tubulin and presumably the MT cytoskeleton and mitochondria in the cytosol of interphase cells that may also occur at least in metaphase during mitosis. Association with the cytoskeleton is consistent with the characteristic ARM- and HEAT-like α-helical repeat structure and the ENTH- and SEC1-domain homology most commonly found in proteins involved in organelle trafficking and major cytoskeletal reorganization events (Liu and McKeehan, 2002). Both cytosolic C19ORF5 and UXT are candidates for MT binding based on sequence homology. C19ORF5 shares primary sequence homology with MT-associated proteins both in its N- and C-terminal domains (CTD) (Liu and McKeehan, 2002). C-terminal residues 450 to 540 of C19ORF5 are homologous to residues 2210 to 2336 of MAP1B, which have been demonstrated to interact directly with MT (Togel et al., 1998). Residues 17 to 149 of 157-residue UXT constitute a DUF232 structural domain similar to that constituted by residues 12 to 142 of the 154-residue subunit 5 of prefoldin. Through hydrophobic residues from the coiled coil structure of DUF232, prefoldin interacts directly with specific sites on nascent α- and βtubulin. The interaction facilitates transfer to c-chaperonin in the process of biogenesis of tubulin into quaternary MT structures (Siegert et al., 2000; Lopez-Fanarraga et al., 2001; Hartl and Hayer-Hartl, 2002). Although the colocalization of LRPPRC with C19ORF5 and UXT does not verify the direct association of LRPPRC indicated by the yeast two-hybrid capture, the fact that overexpression of both C19ORF5 and UXT affects cellular distribution of LRPPRC suggests a functional relationship.

Microtubules are the major component of cytoskeletal systems that underpin mitochondrial transport and homeostasis in mammalian cells (Heggeness et al., 1978), which is achieved through motor proteins as plus-end–directed kinesin and minus-end–directed dynein (Hirokawa, 1998). Microtubule stabilizer, taxol, induced accumulation of mitochondria and mitochondrial DNA (mtDNA) replication, whereas destabilizer, nocodazole, inhibited mitochondrial mass increase and mtDNA replication (Karbowski et al., 2001). Microtubule-associated proteins, such as MAP2, tau, and MAP4, generally stabilize MT tracks (Ebneth et al., 1998) or regulate the attachment or detachment of organelles to the tracks (Trinczek et al., 1999). KIF1B, an MT plus-end–directed monomeric motor protein for transport of mitochondria, is localized in mitochondria (Nangaku et al., 1994). Our current results, together with homology of LRPPRC structural modules and substrates to integrators of organelle trafficking (Liu and McKeehan, 2002), suggest that the LRPPRC complex may be involved in mitochondrial trafficking controlled by the MT cytoskeleton. It is noteworthy that overexpression of the MAP1B homologue, C19ORF5, revealed the distinct mitochondrial punctate staining pattern and overlap of LRPPRC with it in COS7 cells, similar to the MT stabilizer, taxol. This may indicate less sensitivity of the mitochondria–MT association and LRPPRC in the process to MT turnover and dynamics compared with non-mitochondrial MT arrays with associated LRPPRC. This suggests a selective role of C19ORF5 in the former process. Relative differences in the two types of LRPPRC–MT associations may be a fundamental difference among cell types, as illustrated here for COS7 and HepG2 cells. COS7 cells, which have mostly characteristics of mesenchymal-derived cells, are extremely motile and migratory relative to HepG2 cells, whose properties are most like liver parenchymal hepatocytes. In contrast to C19ORF5, overexpression of CECR2B and UXT appeared to amplify the organization of LRPPRC with arrays of MT rather than the punctate pattern.

Nuclear association and bridges to chromatin

Although cytosolic LRPPRC appears predominantly associated with the MT cytoskeleton because of its colocalization with β-tubulin and mitochondria in the cytosol, and primary

substrates UXT and C19ORF5 also appear in the cytosol, primary SEC1 domain substrate CECR2B was strictly nuclear associated. The precise overlap of the signal from the N-terminal GFP tag on CECR2B with DNA stain suggests that CECR2B may be solely within the nucleus rather than associated with it. It is clear that LRPPRC associates with nuclear components during mitosis in the absence of the nuclear boundary (Fig. 2), and nuclear association of LRPPRC was enhanced in interphase COS7 cells transfected with UXT and C19ORF5 (Fig. 4). Although it is unclear how much of the latter is within the nucleus, to access nuclear CECR2B in interphase cells, cytosolic LRPPRC must translocate to an internal nuclear location. Whether LRPPRC or distinct subdomains of it translocate through the nuclear membrane in interphase cells needs further clarification and is under investigation. It is noteworthy that GFP fluorescence occurs in only COS7 cells exhibiting the predominantly cytosolic LRPPRC antigen (type I pattern) when transfected with full-length recombinant LRPPRC labeled at the N terminus. This may suggest exclusion of the N terminus of LRPPRC from the nucleus. We have noted multiple but similar site-specific N-terminal truncations of full-length LRPPRC in yeast, insect, and mammalian cell expression systems. Whether distinct LRPPRC subdomains labeled with GFP at the N or C terminus differentially distribute between cytosol and nucleus is under study.

CECR2B is a splice variant from the *CECR2* gene, which is one of the few expressed sequences that map within the region near the human chromosome 22 pericentromere, a region linked to the multiphenotypes exhibited by cat eye syndrome (Liu and McKeehan, 2002). A part of CECR2B exhibits homology to structural modules of guanylate binding protein 1 (GBP1), a member of the larger family of large GTP-binding proteins involved in MT dynamics and vesicular trafficking. CECR2 exhibits an AT-hook motif next to two bromodomains that are common to chromatin-associated proteins involved in remodeling chromosome structure and regulating gene expression (Liu and McKeehan, 2002). We showed here that CECR2B interacts directly with strictly nuclear, chromatin-associated factors TAFII30 and SRP40. TAFII30 is a high-mobility group 1 (HMG-1) protein, appears in a distinct subset of TBP-associated transcription initiation complexes of the TFIID class, and is required for estrogen receptor–mediated transcriptional activation in vitro (Jacq et al., 1994). Embryonal carcinoma cells lacking TAFII30 are blocked in the G_1/G_0 phase of the cell cycle, undergo high rates of apoptosis, and exhibit defective retinoic acid–induced differentiation (Metzger et al., 1999). SRP40 is a member of the phosphonucleoprotein SR family of pre-mRNA splicing factors that exhibit a characteristic serine-arginine–rich (RS) region in the C terminus (Du et al., 1997). SRP40 plays roles in both basal pre-mRNA splicing and specific alternative splicing in a concentration-dependent mode. SRP40 associates with the hyperphosphorylated CTD of the large subunit of RNA polymerase II during transcription elongation (Smith and Valcarcel, 2000). It is a delayed early gene during the regenerative response in liver and is induced about fivefold during the process (Du et al., 1998). Interaction with these strictly nuclear-associated substrates is consistent with the strictly nuclear location of the CECR2B gene product. Our results in the current report show a precise colocalization of CECR2B with condensed chromatin in apoptotic nuclei that appear as a consequence of over-expression of CECR2B (Fig. 6). This strongly suggests that CECR2B is a chromatin-associated protein that may be involved in condensation and destruction of DNA during nuclear apoptosis. Whether the association is a consequence of the AT hook and bromodomains and chromatin-associated substrates TAFII30 and SRP40, remains to be established.

In addition to its likely association with the MT cytoskeleton in the cytosol, GFP-tagged full-length, 157-residue UXT exhibited an intense nuclear association suggestive of both peri- and intranuclear locations. In addition to its notable α-helical structure within the DUF232 domain, one helical region of UXT is homologous to the basic DNA-binding bHLH-ZIP of SREBP1 and part of the four-helix bundle of transcription factor STAT3b

(Liu and McKeehan, 2002). Except for LRPPRC, interactive substrates of UXT identified in the current study are strictly nuclear. Virtually, all endogenous CITED2 is bound to the CH1 region of p300/CBP in vivo that appears to block access to other CH1 domain-binding transcriptional factors (Goodman and Smolik, 2000). In hypoxic cells, the CITED2 blockade prevents transactivation by HIF-1 by control of access to p300/CBP, thus controlling transcription of hypoxia-induced genes (Goodman and Smolik, 2000). Mice lacking CITED2 display cardiac malformations, adrenal agenesis, neural crest defects, and exencephaly (Bamforth et al., 2001). UXT also interacts with the human homologue of the nuclear, kinetochore-associated checkpoint protein BUB3. BUB3 is a hub for interactions among kinetochore checkpoint proteins, both on and off the kinetochore, that are essential to prevent cells with unaligned chromosomes from prematurely exiting mitosis (Sudakin et al., 2001). BUB3 is notably associated with the kinetochore of lagging chromosomes (Martinez-Exposito et al., 1999). The disruption of BUB3 in mice results in failure of mitotic arrest and massive chromosome abnormalities that are embryonic lethal (Kalitsis et al., 2000). Taken together, these results suggest that the MT cytoskeleton- and mitochondria-associated cytosolic LRPPRC may acquire a nuclear location that then bridges through its primary substrates CECR2B and UXT to key chromatin-associated factors. These factors are involved in both regulation of transcription and chromosome remodeling and fidelity during mitosis. After nuclear dissolution during mitosis, LRPPRC exhibits a distinct distribution at each mitotic phase in relation to separating chromatids that further support its role in chromosome remodeling and cytokinesis.

MT-associated protein homologue C19ORF5, RASSF1, and tumor suppression through apoptosis

Primary LRPPRC substrate C19ORF5 appeared predominantly cytosolic in most cells and, along with cytosolic LRPPRC, generally colocalized with β-tubulin, strongly indicative of a selective association with the MT cytoskeleton. This was consistent with the prediction based on homology of the N- and C-terminal halves of C19ORF5 to sequences in both the N and C termini of much longer MAPs (Liu and McKeehan, 2002). The first 114 residues of C19ORF5 display 41% identity with the region covering residues 121 to 399 of rat MAP1A and regions 188 to 331 of electromotor neuron–associated protein 1 from *Torpedo california*. C-terminal residues 323 to 672 share a 37 to 40% identity with the C terminus of neuronal MAPs. The majority of the cells overexpressing C19ORF5 exhibited a striking increase in nuclear-associated LRPPRC without a coincident increase in C19ORF5 that may indicate a role for C19ORF5 in translocation of LRPPRC to or into the nucleus. Appearance of C19ORF5 at or in the nucleus was associated with cells exhibiting signs of apoptotic degeneration but was distinct from that described above for nuclear resident CECR2B. Instead of the precise overlap and colocalization with condensed DNA exhibited by CECR2B, C19ORF5 appeared to encircle or remain on the periphery of condensed DNA at different stages of disintegration until it disappeared altogether.

Yeast two-hybrid capture revealed a potential association between C19ORF5 and candidate tumor suppressor RASSF1. RASSF1 was first identified by capture in a yeast two-hybrid screen with human DNA repair protein XPA as the snare (Dammann et al., 2000). Three alternatively spliced transcripts (RASSF1A, B, and C) arise from the *RASSF1* gene within locus 3p21.3 (Dammann et al., 2000). All three products share the Ras association (RalGDS/AF-6) domain in the C terminus, whereas RASSF1A uniquely exhibits an N-terminal cysteine-rich diacylglycerol-phorbol ester–binding domain (protein kinase C C1 domain). Loss of heterozygosity at 3p21.3 and loss of expression of specifically RASSF1A accompanied by specific hypermethylation of CpG islands in the RASSF1A promoter occur in a significant portion of tumors and tumor cell lines: lung (Dammann et al., 2000; Agathanggelou et al., 2001; Burbee et al., 2001; Dammann et al., 2001a), breast

(Agathanggelou et al., 2001; Burbee et al., 2001; Dammann et al., 2001b), prostate (Kuzmin et al., 2002), bladder (Lee et al., 2001), nasopharyngeal (Lo et al., 2001), gastric (Byun et al., 2001), renal (Dreijerink et al., 2001; Morrissey et al., 2001; Yoon et al., 2001), head and neck (Hasegawa et al., 2002), thyroid (Schagdarsurengin et al., 2002), SV40-infected mesotheliomas (Toyooka et al., 2001), ovarian (Agathanggelou et al., 2001; Yoon et al., 2001), neural crest adenocarcinomas (Astuti et al., 2001), and medulloblastoma, rhabdomyosarcoma, retinoblastoma, neuroblastoma, and Wilms' tumors (Harada et al., 2002). Notably, HepG2 cells exhibited a smaller transcript of about 1.5 kb of RASSF1A compared with the 1.8-kb transcript exhibited by most cells (Dammann et al., 2000). Vos et al. (2000) reported that RASSF1 bound Ras in a GTP-dependent manner in vivo and in vitro and that activated Ras enhanced RASSF1-induced apoptosis, whereas inhibition of Ras abrogated the RASSF1 effect. The significance of the direct interaction of RASSF1 with Ras has been questioned with the demonstration that RASSF1A may bind Ras indirectly by heterodimerization with high-affinity Ras-binding Nore1 (Ortiz-Vega et al., 2002). A subsequent study further demonstrated that RASSF1, similar to Nore1, forms a stable complex with the proapoptotic and potential tumor suppressor, Ste20-related protein kinase MST1, with potential for recruitment by Ras in Ras-induced apoptosis (Khokhlatchev et al., 2002). Nuclear translocation of MST1 correlates with caspase cleavage of MST1, chromatin condensation, and disintegration of nuclei (Ura et al., 2001). A more recent report contended that specifically RASSF1A induced G1 cell cycle arrest coincident with inhibition of cyclin D1 and could not be overridden by oncogenic Ras (Shivakumar et al., 2002). Moreover, the same authors showed that no apoptosis was evident in cells overexpressing recombinant RASSF1A or RASSF1C as reported by others (Vos et al., 2000). Independent of the precise mechanism of RASSF1 action, our observations link the LRPPRC complex through its primary substrate C19ORF5 to RASSF1 and, thus, potentially apoptotic signaling and tumor suppression mechanisms that occur in both cytosolic and nuclear compartments.

The potential link of the LRPPRC complex to mitochondrial function and potentially mitochondria-mediated apoptosis through C19ORF5 was further strengthened by the association of LRPPRC with mitochondria and the interaction of its primary substrate C19ORF5 with inner-membrane proteins NADH dehydrogenase I (NAD1) and COX1 in the yeast two-hybrid capture system. In addition to fueling healthy cells, mitochondria and mitochondrial permeability play a central role in cell death by both apoptosis and necrosis (Kroemer et al., 1998; Ravagnan et al., 2002; Waterhouse et al., 2002). It is noteworthy that, similar to NAD1, the interferon-β and retinoic acid–induced cell death regulatory protein GRIM-19 appear to be an integral subunit of the NADH–ubiquinone oxidoreductase complex I (Fearnley et al., 2001). Whether the C19ORF5 interaction plays a net positive or negative role in preservation of mitochondrial function or apoptosis after outer-membrane permeabilization requires clarification (Waterhouse et al., 2002). Our results demonstrate that the LRPPRC complex is not only in a position to play a key role in distribution of mitochondria by the MT cytoskeleton in healthy cellular processes where aden-osine triphosphate is needed most but also to position mitochondria at sites of critical function as chromosome remodeling where error triggers mitochondrial-mediated cell death.

Hypothetical model and function of a nucleocytosolic LRPPRC complex

Here, we showed that the cellular localization in cultured cells in vitro of LRPPRC and primary and secondary substrates identified by yeast two-hybrid capture are compatible with predictions of sequence homology and the diverse complexes from multiple cell compartments in cell extracts from which LRPPRC has been reported (Liu and McKeehan, 2002). Figure 9 illustrates a hypothetical model of the LRPPRC complex in interphase cytosol and nuclei and during mitosis (metaphase–anaphase), taking into consideration all data to date. Whether the indicated interactions occur concurrently or are mutually exclusive

or competitive is under investigation. We propose that LRPPRC through C19ORF5 and possibly direct or other indirect molecular bridges associates with both the MT cytoskeleton and mitochondria, which may contribute to alignment of mitochondria with the MT cytoskeleton both in inter-phase cytosol and mitosis. If the outer mitochondrial membrane is breached during apoptotic permeability transition, C19ORF5 has potential to interact with subunits NAD1 and COX1 of oxidative complexes I and IV, respectively, on the inner membrane. LRPPRC, or a portion of it, may translocate to the nucleus alone or carry cytosolic substrates UXT and C19ORF5 that also appear nuclear associated in some cells. The nuclear LRPPRC–UXT–CECR2B complex potentially communicates with the basal transcription apparatus at three points through CITED2, TAFII30, and SRP40 to affect gene expression. These associations may be stimulatory or quenching for transcription, and cell growth and differentiation or serve simply as bridges to chromatin. The LRPPRC complex appears to potentially participate in chromosome separation and fidelity of the process during mitosis that includes communication with the chromatid kinetochore through BUB3. The LRPPRC complex conceivably links cytoskeletal integrity and mitochondria-mediated apoptosis in interphase cytosol and nuclear apoptosis through C19ORF5 and CECR2B in interphase nuclei. However, of potentially more importance, we propose a role for the complex in critical mitotic events that include chromosome separation and cytokinesis and bridging of mitochondria to them. This may include a role in concurrently concentrating healthy mitochondria at the site and partitioning them between daughter cells, but it is most important to poise them for initiation of apoptosis in the event of error. RASSF1 provides the potential bridge for the LRPPRC complex to apoptotic tumor suppression in a wide variety of human neoplasms. Detailed colocalization analysis beyond the scope of this study of RASSF1 is still in progress, and the results will be the subject of a future report. Preliminary results indicate that overexpressed GFP-labeled RASSF1C appears predominantly in the cytosol of interphase COS7 cells, associates with the MT cytoskeleton, and causes notable bundling of fibrils containing β-tubulin that encircle the nuclei. This pattern has been recently reported for overexpressed myc-tagged RASSF1A in several cultured epithelial cell types (Shivakumar et al., 2002).

This network of interactions deduced by a combination of sequence analysis in silico using the human genome sequence database, interaction cloning in yeast, and colocalization analysis in vitro defines a hypothetical LRPPRC complex. The results provide a framework for validation of the complex and hypothetical pathway and characterization of the individual aspects of the role and regulation of the complex in cytoskeletal organization, mitochondria trafficking, chromosome remodeling, apoptosis, and tumor suppression. This does not preclude the roles of individual LRPPRC structural domains and primary and secondary substrates in nucleocytosolic shuttling, cell organelle and cytoskeletal remodeling, or transcriptional processes not shown here. Mili et al. (2001) have identified LRPPRC as a prominent component of ribonucleoprotein complexes containing a subset of proteins involved in maturation and export of nuclear mRNA. LRPPRC binds and crosslinks to poly A–containing mRNA apparently through a novel type of RNA-binding domain (Mili et al., 2001). Consistent with the nuclear appearance of LRPPRC and association with diverse nucleic acid complexes from cell extracts, Tsuchiya et al. (2002) recently reported the interaction of LRPPRC with single-stranded cytosine-rich sequences of mouse hypervariable minisatellite Pc-1.

The modular structure, cytoskeletal association, multicompartment localization, nucleocytosolic trafficking, link to apoptosis and tumor suppression, and diversity and characteristics of primary and secondary interactive substrates of LRPPRC exhibit numerous parallels to the adenomatous polyposis coli (APC) family (Kaplan et al., 2001; Zumbrunn et al., 2001). It will be important to determine whether the LRPPRC complex and its functions are coupled to specific signaling pathways similar to the relationship between APC and the

Wnt signaling pathway. LRPPRC was first detected and its structure determined from extracts enriched in ligand-labeled FGFR signaling complexes (DiSorbo et al., 1988; Hou et al., 1994).

Acknowledgments

We thank Dr. Serafín Piñol-Roma, Mount Sinai School of Medicine, New York, for mouse monoclonal antibody against LRPPRC and for helpful discussions. This work was supported by Public Health Service Grants DK35310 and DK47039 from NIDDK and CA59971 from NCI, National Institutes of Health.

References

Agathanggelou A, Honorio S, Macartney DP, et al. Methylation associated inactivation of RASSF1A from region 3p21.3 in lung, breast and ovarian tumours. Oncogene. 2001; 20:1509–1518. [PubMed: 11313894]

Astuti D, Agathanggelou A, Honorio S, et al. RASSF1A promoter region CpG island hypermethylation in phaeochromocytomas and neuroblastoma tumours. Oncogene. 2001; 20:7573–7577. [PubMed: 11709729]

Bamforth SD, Braganca J, Eloranta JJ, et al. Cardiac malformations, adrenal agenesis, neural crest defects and exencephaly in mice lacking Cited2, a new Tfap2 co-activator. Nat. Genet. 2001; 29:469–474. [PubMed: 11694877]

Bhattacharya S, Michels CL, Leung MK, et al. Functional role of p35srj, a novel p300/CBP binding protein, during transactivation by HIF-1. Genes Dev. 1999; 13:64–75. [PubMed: 9887100]

Burbee DG, Forgacs E, Zochbauer-Muller S, et al. Epigenetic inactivation of RASSF1A in lung and breast cancers and malignant phenotype suppression. J. Natl. Cancer Inst. 2001; 93:691–699. [PubMed: 11333291]

Byun DS, Lee MG, Chae KS, et al. Frequent epigenetic inactivation of RASSF1A by aberrant promoter hypermethylation in human gastric adenocarcinoma. Cancer Res. 2001; 61:7034–7038. [PubMed: 11585730]

Collins TJ, Berridge MJ, Lipæp P, Bootman MD. Mitochondria are morphologically and functionally heterogeneous within cells. EMBO J. 2002; 21:1616–1627. [PubMed: 11927546]

Dammann R, Li C, Yoon JH, et al. Epigenetic inactivation of a RAS association domain family protein from the lung tumour suppressor locus 3p21.3. Nat. Genet. 2000; 25:315–319. [PubMed: 10888881]

Dammann R, Takahashi T, Pfeifer GP. The CpG island of the novel tumor suppressor gene RASSF1A is intensely methylated in primary small cell lung carcinomas. Oncogene. 2001a; 20:3563–3567. [PubMed: 11429703]

Dammann R, Yang G, Pfeifer GP. Hypermethylation of the cpG island of Ras association domain family 1A (RASSF1A), a putative tumor suppressor gene from the 3p21.3 locus, occurs in a large percentage of human breast cancers. Cancer Res. 2001b; 61:3105–3109. [PubMed: 11306494]

DiSorbo D, Shi E, McKeehan W. Purification form human hepatoma cells of a 130-kDa membrane glycoprotein with properties of the heparin-binding growth factor receptor. Biochem. Biophys. Res. Commun. 1988; 157:1007–1014. [PubMed: 2462864]

Dreijerink K, Braga E, Kuzmin I, et al. The candidate tumor suppressor gene, RASSF1A, from human chromosome 3p21.3 is involved in kidney tumorigenesis. Proc. Natl. Acad. Sci. USA. 2001; 98:7504–7509. [PubMed: 11390984]

Du K, Leu JI, Peng Y, Taub R. Transcriptional up-regulation of the delayed early gene HRS/SRp40 during liver regeneration. Interactions among YY1, GA-binding proteins, and mitogenic signals. J. Biol. Chem. 1998; 273:35208–35215. [PubMed: 9857059]

Du K, Peng Y, Greenbaum LE, et al. HRS/SRp40-mediated inclusion of the fibronectin EIIIB exon, a possible cause of increased EIIIB expression in proliferating liver. Mol. Cell. Biol. 1997; 17:4096–4104. [PubMed: 9199345]

Ebneth A, Godemann R, Stamer K, et al. Overexpression of tau protein inhibits kinesin-dependent trafficking of vesicles, mitochondria, and endoplasmic reticulum: implications for Alzheimer's disease. J. Cell Biol. 1998; 143:777–794. [PubMed: 9813097]

Fearnley IM, Carroll J, Shannon RJ, et al. GRIM-19, a cell death regulatory gene product, is a subunit of bovine mitochondrial NADH:ubiquinone oxidoreductase (complex I). J. Biol. Chem. 2001; 276:38345–38348. [PubMed: 11522775]

Fields S, Song O. A novel genetic system to detect protein-protein interactions. Nature. 1989; 340:245–246. [PubMed: 2547163]

Ghiso NS, Lennon GG. lrp130 Gene assigned to chromosome 2. In Vitro Cell. Dev. Biol. 1994; 30A: 744.

Goodman R, Smolik S. CBP/p300 in cell growth, transformation, and development. Genes Dev. 2000; 14:1553–1577. [PubMed: 10887150]

Goold RG, Gordon-Weeks PR. Microtubule-associated protein 1B phosphorylation by glycogen synthase kinase 3beta is induced during PC12 cell differentiation. J. Cell Sci. 2001; 114:4273–4284. [PubMed: 11739659]

Harada K, Toyooka S, Maitra A, et al. Aberrant promoter methylation and silencing of the RASSF1A gene in pediatric tumors and cell lines. Oncogene. 2002; 21:4345–4349. [PubMed: 12082624]

Hartl FU, Hayer-Hartl M. Molecular chaperones in the cytosol: from nascent chain to folded protein. Science. 2002; 295:1852–1858a. [PubMed: 11884745]

Hasegawa M, Nelson HH, Peters E, et al. Patterns of gene promoter methylation in squamous cell cancer of the head and neck. Oncogene. 2002; 21:4231–4236. [PubMed: 12082610]

Hatefi Y. The mitochondrial electron transport and oxidative phosphorylation system. Annu. Rev. Biochem. 1985; 54:1015–1069. [PubMed: 2862839]

Heggeness MH, Simon M, Singer SJ. Association of mitochondria with microtubules in cultured cells. Proc. Natl. Acad. Sci. USA. 1978; 75:3863–3866. [PubMed: 80800]

Hirokawa N. Kinesin and dynein superfamily proteins and the mechanism of organelle transport. Science. 1998; 279:519–526. [PubMed: 9438838]

Hou J, Wang F, McKeehan WL. Molecular cloning and expression of the gene for a major leucine-rich protein from human hepatoblastoma cells (HepG2). In Vitro Cell. Dev. Biol. 1994; 30A:111–114.

Jacq X, Brou C, Lutz Y, et al. Human TAFII30 is present in a distinct TFIID complex and is required for transcriptional activation by the estrogen receptor. Cell. 1994; 79:107–117. [PubMed: 7923369]

Kalitsis P, Earle E, Fowler KJ, Choo KH. Bub3 gene disruption in mice reveals essential mitotic spindle checkpoint function during early embryogenesis. Genes Dev. 2000; 14:2277–2282. [PubMed: 10995385]

Kaplan KB, Burds AA, Swedlow JR, et al. A role for the adenomatous polyposis coli protein in chromosome segregation. Nat. Cell Biol. 2001; 3:429–432. [PubMed: 11283619]

Karbowski M, Spodnik JH, Teranishi M, et al. Opposite effects of microtubule-stabilizing and microtubule-destabilizing drugs on biogenesis of mitochondria in mammalian cells. J. Cell Sci. 2001; 114:281–291. [PubMed: 11148130]

Khokhlatchev A, Rabizadeh S, Xavier R, et al. Identification of a novel ras-regulated proapoptotic pathway. Curr. Biol. 2002; 12:253–265. [PubMed: 11864565]

Kroemer G, Dallaporta B, Resche-Rigon M. The mitochondrial death/life regulator in apoptosis and necrosis. Annu. Rev. Physiol. 1998; 60:619–642. [PubMed: 9558479]

Kuzmin I, Gillespie JW, Protopopov A, et al. The RASSF1A tumor suppressor gene is inactivated in prostate tumors and suppresses growth of prostate carcinoma cells. Cancer Res. 2002; 62:3498–3502. [PubMed: 12067994]

Lee MG, Kim HY, Byun DS, et al. Frequent epigenetic inactivation of RASSF1A in human bladder carcinoma. Cancer Res. 2001; 61:6688–6692. [PubMed: 11559536]

Li H, Kolluri SK, Gu J, et al. Cytochrome c release and apoptosis induced by mitochondrial targeting of nuclear orphan receptor TR3. Science. 2000; 289:1159–1164. [PubMed: 10947977]

Liu L, McKeehan WL. Sequence analysis of LRPPRC and its SEC1 domain interaction partners suggest roles in cytoskeletal organization, vesicular trafficking, nucleocytosolic shuttling and chromosome activity. Genomics. 2002; 79:124–136. [PubMed: 11827465]

Lo KW, Kwong J, Hui AB, et al. High frequency of promoter hypermethylation of RASSF1A in nasopharyngeal carcinoma. Cancer Res. 2001; 61:3877–3881. [PubMed: 11358799]

Longman D, Johnstone IL, Caceres JF. Functional characterization of SR and SR-related genes in Caenorhabditis elegans. EMBO J. 2000; 19:1625–1637. [PubMed: 10747030]

Lopez-Fanarraga M, Avila J, Guasch A, et al. Review: postchaperonin tubulin folding cofactors and their role in microtubule dynamics. J. Struct. Biol. 2001; 135:219–229. [PubMed: 11580271]

Martinez-Exposito MJ, Kaplan KB, Copeland J, Sorger PK. Retention of the BUB3 checkpoint protein on lagging chromosomes. Proc. Natl. Acad. Sci. USA. 1999; 96:8493–8498. [PubMed: 10411903]

Metzger D, Scheer E, Soldatov A, Tora L. Mammalian TAFII30 is required for cell cycle progression and specific cellular differentiation programmes. EMBO J. 1999; 18:4823–4834. [PubMed: 10469660]

Mili S, Shu HJ, Zhao Y, Pinol-Roma S. Distinct RNP complexes of shuttling hnRNP proteins with pre-mRNA and mRNA: candidate intermediates in formation and export of mRNA. Mol. Cell. Biol. 2001; 21:7307–7319. [PubMed: 11585913]

Morrissey C, Martinez A, Zatyka M, et al. Epigenetic inactivation of the RASSF1A 3p21.3 tumor suppressor gene in both clear cell and papillary renal cell carcinoma. Cancer Res. 2001; 61:7277–7281. [PubMed: 11585766]

Nangaku M, Sato-Yoshitake R, Okada Y, et al. KIF1B, a novel microtubule plus end-directed monomeric motor protein for transport of mitochondria. Cell. 1994; 79:1209–1220. [PubMed: 7528108]

Ortiz-Vega S, Khokhlatchev A, Nedwidek M, et al. The putative tumor suppressor RASSF1A homodimerizes and heterodimerizes with the Ras-GTP binding protein Nore1. Oncogene. 2002; 21:1381–1390. [PubMed: 11857081]

Ravagnan L, Roumier T, Kroemer G. Mitochondria, the killer organelles and their weapons. J. Cell Physiol. 2002; 192:131–137. [PubMed: 12115719]

Ruitenberg M, Kannt A, Bamberg E, et al. Reduction of cytochrome c oxidase by a second electron leads to proton translocation. Nature. 2002; 417:99–102. [PubMed: 11986672]

Schagdarsurengin U, Gimm O, Hoang-Vu C, et al. Frequent epigenetic silencing of the CpG island promoter of RASSF1A in thyroid carcinoma. Cancer Res. 2002; 62:3698–3701. [PubMed: 12097277]

Shivakumar L, Minna J, Sakamaki T, et al. The RASSF1A tumor suppressor blocks cell cycle progression and inhibits cyclin D1 accumulation. Mol. Cell. Biol. 2002; 22:4309–4318. [PubMed: 12024041]

Siegert R, Leroux MR, Scheufler C, et al. Structure of the molecular chaperone prefodin: unique interaction of multiple coiled coil tentacles with unfod ed proteins. Cell. 2000; 103:621–632. [PubMed: 11106732]

Smith CW, Valcarcel J. Alternative pre-mRNA splicing: the logic of combinatorial corol. Trends Biochem. Sci. 2000; 25:381–388. [PubMed: 10916158]

Sudakin V, Chan GK, Yen TJ. Checkpoint inhibition of the APC/C in HeLa cells is mediated by a complex of BUBR1, BUB3, CDC20, and MAD2. J. Cell Biol. 2001; 154:925–936. [PubMed: 11535616]

Suzuki Y, Wanaka A, Tohyama M, Takagi T. Identification of differentially expressed mRNAs during neuronal differentiation of P19 embryonal carcinoma cells. Neurosci. Res. 1995; 23:65–71. [PubMed: 7501302]

Thornton JM. From genome to function. Science. 2001; 292:2095–2097. [PubMed: 11408660]

Togel M, Wiche G, Propst F. Novel features of the light chain of microtubule-associated protein MAP1B: microtubule stabilization, self interaction, actin filament binding, and regulation by the heavy chain. J. Cell Biol. 1998; 143:695–707. [PubMed: 9813091]

Toyooka S, Pass HI, Shivapurkar N, et al. Aberrant methylation and simian virus 40 tag sequences in malignant mesothelioma. Cancer Res. 2001; 61:5727–5730. [PubMed: 11479207]

Trinczek B, Ebneth A, Mandelkow EM, Mandelkow E. Tau regulates the attachment/detachment but not the speed of motors in microtubule-dependent transport of single vesicles and organelles. J. Cell Sci. 1999; 112(Part 14):2355–2367. [PubMed: 10381391]

Tsuchiya N, Fukuda H, Sugimura T, et al. LRP130, a protein containing nine pentatricopeptide repeat motifs, interacts with a single-stranded cytosine-rich sequence of mouse hypervariable minisatellite Pc-1. Eur. J. Biochem. 2002; 269:2927–2933. [PubMed: 12071956]

Ura S, Masuyama N, Graves JD, Gotoh Y. Caspase cleavage of MST1 promotes nuclear translocation and chromatin condensation. Proc. Natl. Acad. Sci. USA. 2001; 98:10148–10153. [PubMed: 11517310]

Vos MD, Ellis CA, Bell A, et al. Ras uses the novel tumor suppressor RASSF1 as an effector to mediate apoptosis. J. Biol. Chem. 2000; 275:35669–35672. [PubMed: 10998413]

Wang HJ, Guay G, Pogan L, et al. Calcium regulates the association between mitochondria and a smooth subdomain of the endoplasmic reticulum. J. Cell Biol. 2000; 150:1489–1498. [PubMed: 10995452]

Waterhouse NJ, Ricci JE, Green DR. And all of a sudden it's over: mitochondrial outer-membrane permeabilization in apoptosis. Biochimie. 2002; 84:113–121. [PubMed: 12022942]

Yoon JH, Dammann R, Pfeifer GP. Hypermethylation of the CpG island of the RASSF1A gene in ovarian and renal cell carcinomas. Int. J. Cancer. 2001; 94:212–217. [PubMed: 11668500]

Zumbrunn J, Kinoshita K, Hyman AA, Nathke IS. Binding of the adenomatous polyposis coli protein to microtubules increases microtubule stability and is regulated by GSK3 beta phosphorylation. Curr. Biol. 2001; 11:44–49. [PubMed: 11166179]

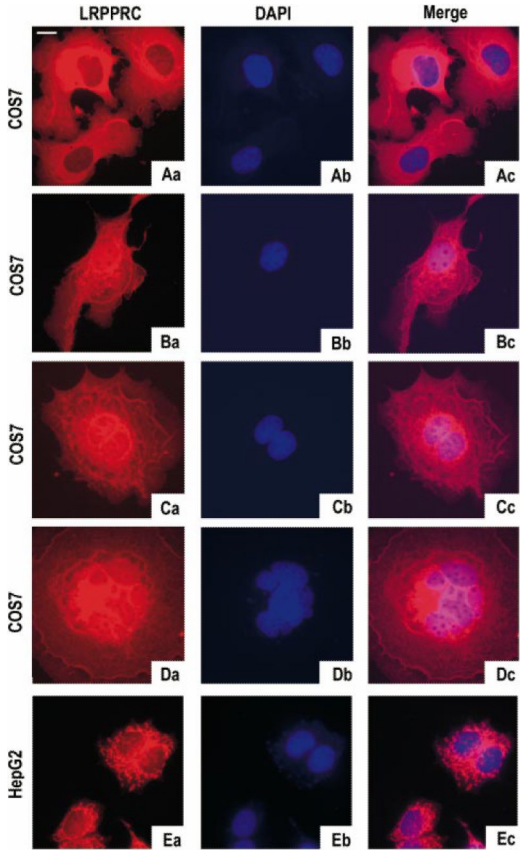

FIG. 1.

Immunochemical analysis of LRPPRC antigen in interphase cells. COS7 (*A–D*) and HepG2 (*E*) cells were cultured, fixed, and incubated with mouse monoclonal antibody Mab4C12 raised against LRPPRC as described in the Materials and Methods. The mouse antibody was detected by Texas Red-X–labeled goat anti-mouse lgG (*red*), and nuclei were stained with DAPI (*blue*). Colors from the *left* and *middle panels* were merged in the *right panel*. *Pink* indicates overlap of the red LRPPRC antibody stain with the blue DAPI DNA stain. *Bar upper left*, 10 μm. LRPPRC, leucine-rich pentatricopeptide repeat-motif–containing complex; DAPI, 4,6-diamidino-2-phenylindole; DNA, deoxyribonucleic acid; HepG2, human hepatoma cells.

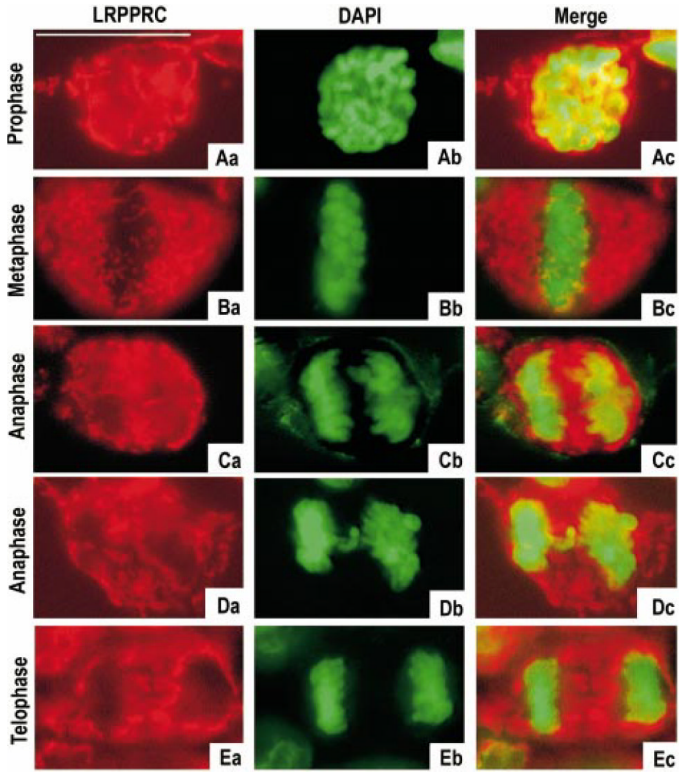

FIG. 2.

Analysis of LRPPRC antigen in mitotic HepG2 cells. The percentage of mitotic HepG2 cells in the cultured population was increased by serum depletion and subsequent addition of 5% serum for 4 h (Materials and Methods). The antigen LRPPRC (*red*) and DNA (*green*) were analyzed as described in Fig. 1. *Bar upper left*, 10 μm. LRPPRC, leucine-rich pentatricopeptide repeat-motif–containing complex; DNA, deoxyribonucleic acid; HepG2, human hepatoma cells.

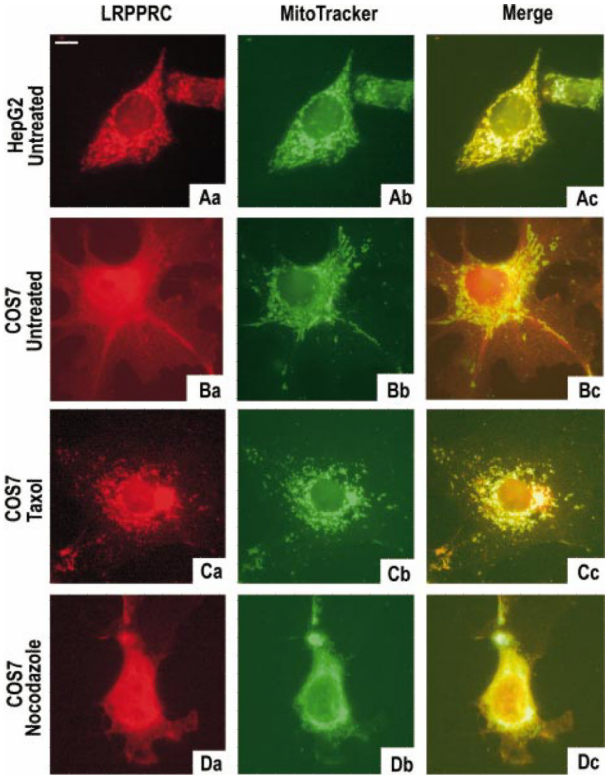

FIG. 3.

Colocalization of LRPPRC antigen with mitochondria in interphase cells. HepG2 (*A*) and COS7 (*B*) cells were labeled for 30 min with 1 μ*M* of MitoTracker® Red CM-H_2XRos (assigned *green*) before fixation and analysis for LRPPRC with Mab4C12 and FITC-conjugated goat anti-mouse-IgG antibody (assigned *red*). COS7 cells were treated with 10 μ*M* taxol or nocodazole overnight before the above analysis as indicated. *Merged yellow* indicates colocalization of LRPPRC antigen and mitochondria. *Bar upper left*, 10 μm. LRPPRC, leucine-rich pentatricopeptide repeat-motif–containing complex; HepG2, human hepatoma cells; FITC, fluorescein isothiocyanate.

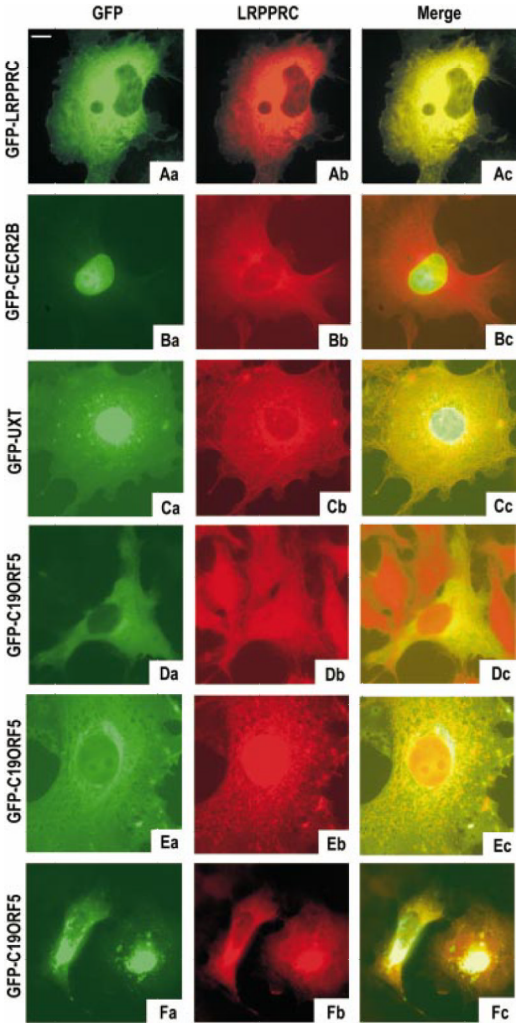

FIG. 4.

Colocalization of recombinant GFP-labeled LRPPRC, CECR2B, UXT, and C19ORF5 with native LRPPRC antigen. COS7 cells were transiently transfected with cDNAs coding for the indicated products labeled with GFP at the N terminus. Cells were stained with Mab4C12 antibody as described in Fig. 1. Product labeled with GFP is indicated in *green* and Mab4C12-stained antigen in *red. Orange* and *yellow* indicate overlap of GFP-labeled product and LRPPRC antigen. *Bar upper left*, 10 μm. GFP, green fluorescent protein; LRPPRC, leucine-rich pentatricopeptide repeat-motif–containing complex; cDNA, complementary deoxyribonucleic acid.

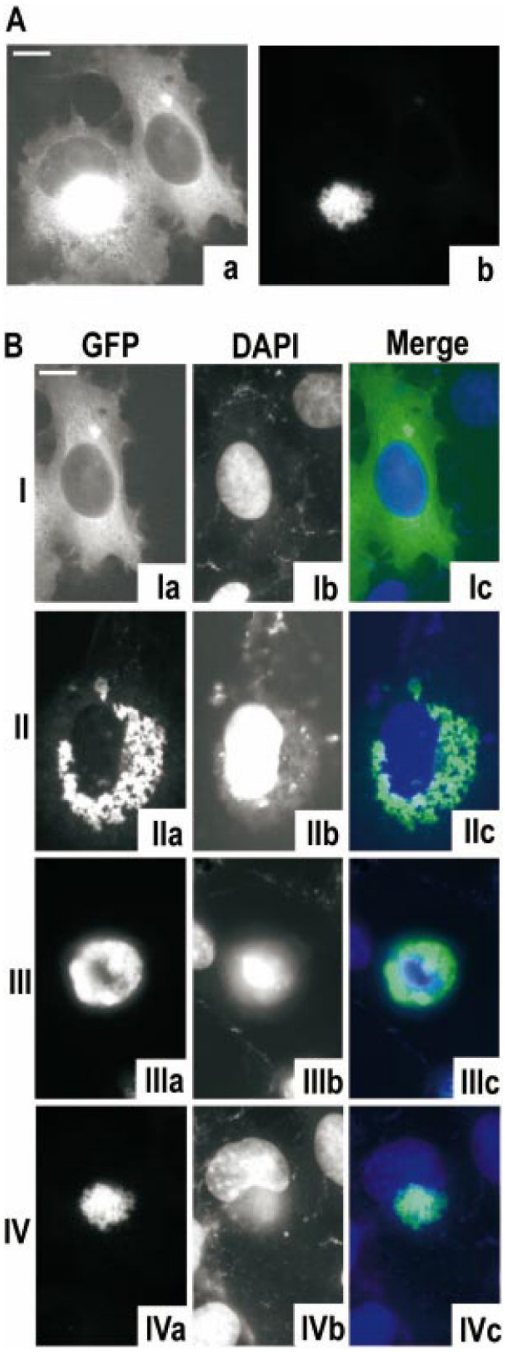

FIG. 5.

Nuclear condensation of GFP–C19ORF5 and disintegration of DNA. COS7 cells were fixed 72 h after transient transfection of GFP–C19ORF5 and counterstained with DAPI. (*A*) Binucleate cell with condensed GFP–C19ORF5 in one nuclei. *a* and *b* are the same fields viewed at a 20-times different sensitivity setting. (*B*) Examples of nuclear condensation of GFP–C19ORF5 coincident with disintegration of DNA. The relative intensity of the GFP signal was 1, 2, 10, and 20 in examples I, II, III, and IV, respectively, whereas the DAPI (DNA) signal intensity was uniform. Individual green GFP and blue DAPI fluorescence is indicated as *white* and *merged*, respectively. *Bar upper left*, 10 μm. GFP, green fluorescent protein; DNA, deoxyribonucleic acid; DAPI, 4,6-diamidino-2-phenylindole.

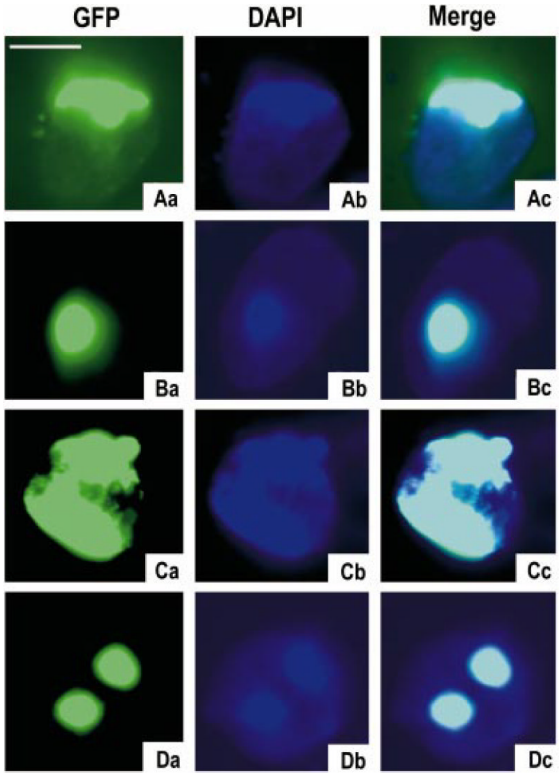

FIG. 6.

Association of condensed GFP–CECR2B with condensed DNA. COS7 cells were fixed 72 h after transfection with GFP–CECR2B (*green*) and stained with DAPI (*blue*). Four different examples in which condensed DNA appears in distinct foci in different parts of the nucleus are indicated. *Cyan* in the *right panel* indicates overlap of the two signals. *Bar upper left*, 10 μm. GFP, green fluorescent protein; DNA, deoxyribonucleic acid; DAPI, 4,6-diamidino-2-phenylindole.

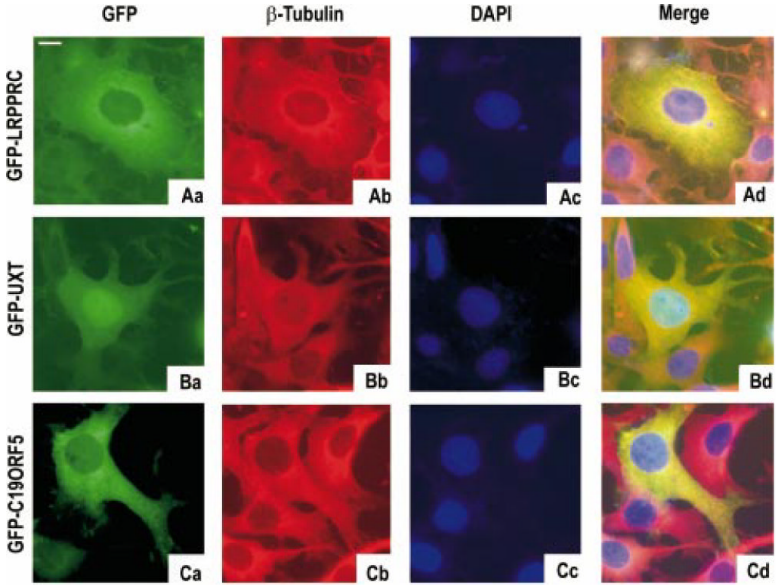

FIG. 7.

Colocalization of GFP-labeled LRPPRC, UXT, and C19ORF5 with the β-tubulin. COS7 cells were transiently transfected with the GFP-labeled product indicated by *green* and then stained with mouse anti-βtubulin (clone TUB 2.1) monoclonal antibody followed by goat Texas Red–conjugated anti-mouse-IgG antibody (*red*). Nuclei were stained with DAPI (*blue*). Colors were merged in the *right panel*, where *yellow* indicated overlap of GFP-labeled products with β-tubulin. *Cyan* indicated overlap of nuclear-associated green GFP with blue DAPI–stained DNA. *Bar upper left*, 10 μm. GFP, green fluorescent protein; LRPPRC, leucine-rich pentatricopeptide repeat-motif–containing complex; DAPI, 4,6-diamidino-2-phenylindole.

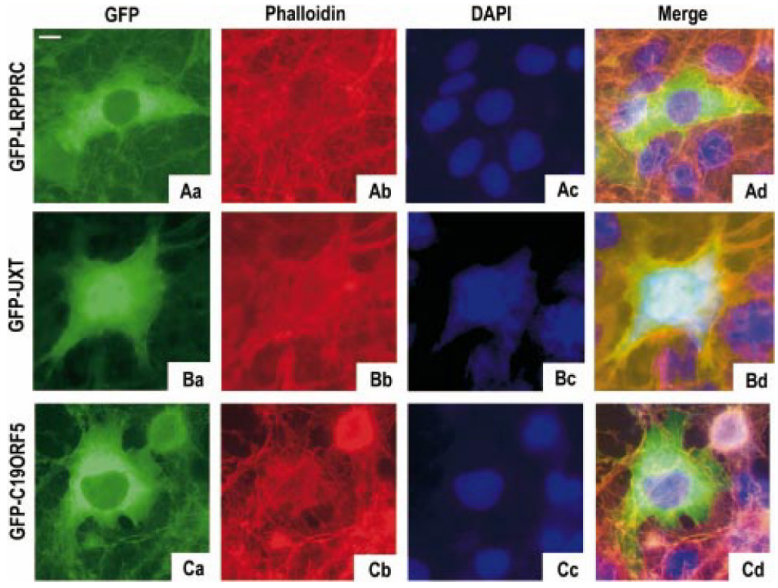

FIG. 8.

Lack of colocalization of GFP-labeled LRPPRC, UXT, and C19ORF5 proteins with the actin cytoskeleton. Cells expressing the same GFP-labeled expression products (*green*) described in Fig. 7 were permeabilized as described in the Materials and Methods. F-actin was stained with Texas Red-X–tagged phalloidin (*red*). Nuclear DNA was stained with DAPI (*blue*). In the *merged panel*, absence of significant *yellow* indicates lack of overlap of GFP-products and F-actin. *Cyan* indicates overlap of GFP and DAPI signals. Image capture was unfiltered to avoid an interfering brown background at 488 nm. This resulted in some artifactual *green background* in the *left panels* and consequently some *yellow* in the *merged panel. Bar upper left*, 10 μm. GFP, green fluorescent protein; LRPPRC, leucine-rich pentatricopeptide repeat-motif–containing complex; DNA, deoxyribonucleic acid; DAPI, 4,6-diamidino-2-phenylindole.

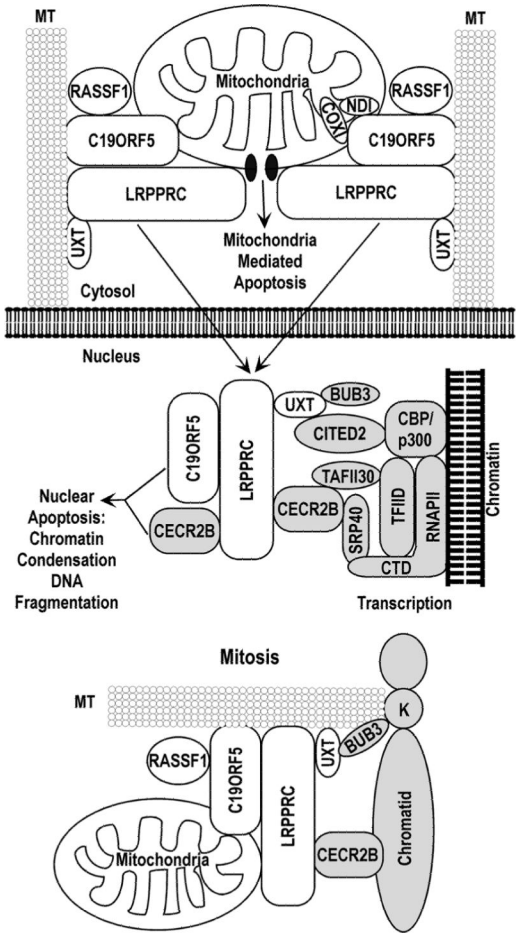

FIG. 9.

Potential identity, interactions, and function of the LRPPRC complex. Potential interactions in interphase cytosol and nucleus plus mitotic metaphase and anaphase are indicated. *Component acronyms* are defined in the text, in Table 1, and below. *Shaded components* indicate a strictly nuclear location in interphase cells. A separated sister chromatid attached to a microtubule (MT) at the kinetochore (K) is depicted in the mitosis schematic. TFIID, subunit of TATA-binding transcription initiation factor; RNAPII, RNA polymerase II; CTD, the C-terminal domain of the large subunit of RNA polymerase I; LRPPRC, leucine-rich pentatricopeptide repeat-motif–containing complex.

TABLE 1

SECONDARY SUBSTRATES CAPTURED BY PRIMARY LRPPRC SUBSTRATES FROM A HUMAN LIVER cDNA LIBRARY BY YEAST TWO-HYBRID SELECTION[a]

Bait	Substrate	Accession no.	Function	Reference
CECR2B	TAFII30	Q12962	Transcription coactivator	Jacq et al., 1994
			Cell cycle progression	Metzger et al., 1999
	SRP40	S59042	Pre-mRNA splicing, cell cycle progression	Longman et al., 2000
			Liver regeneration response	Du et al., 1998
UXT	BUB3	043684	Mitotic checkpoint, kinetochore complex	Sudakin et al., 2001
	CITED2	AAF01263	Transcription coactivator	Bhattacharya et al., 1999
			Binds to p300/CBP, AP-2	Bamforth et al., 2001
C19ORF5	RASSF1C	AAD44175	Tumor suppressor	Dammann et al., 2000
			Apoptosis	Vos et al., 2000
	NADH dehydrogenase I (ND1)	AAL54787	Mitochondrial NADH–ubiquinone oxidoreductase (complex I)	Hatefi, 1985
	Cytochrome *c* oxidase I (COX1)	AAG59851	Mitochondrial oxidoreductase complex IV	Ruitenberg et al., 2002

[a]Abbreviations: LRPPRC, leucine-rich pentatricopeptide repeat-motif–containing complex; cDNA, complementary deoxyribonucleic acid; mRNA, messenger ribonucleic acid; NADH, nicotinamide adenine dinucleotide (reduced).